Current Optics and Photonics
Vol. 3, No. 6, December 2019, pp. 566-570

ISSN: 2508-7266(Print) / ISSN: 2508-7274(Online)
DOI: https://doi.org/10.3807/COPP.2019.3.6.566

Investigation of Sensitivity Distribution in THz Metamaterials Using Surface Functionalization

Sung Ho Cha, Sae June Park, and Yeong Hwan Ahn*

Department of Physics and Department of Energy Systems Research, Ajou University, Suwon 16499, Korea

(Received July 29, 2019 : revised August 27, 2019 : accepted August 29, 2019)

To investigate dependence of the sensitivity of THz metamaterials on the position of target dielectric materials, we functionalized the metamaterial gap with an adhesive polymer. A shift in resonance frequency occurs when polystyrene microbeads are deposited in the gap of the metamaterial's metal resonator pattern, while little change is observed when they are deposited on other areas of the metasurface. A two-dimensional mapping of the sensitivity, with a grid size of 1 μm, is obtained from a finite-difference time-domain simulation: The frequency shift is displayed as a function of the position of a target dielectric cube. The resulting sensitivity distribution clearly reveals the crucial role of the gap in sensing with metamaterials, which is consistent with the electric field distribution near the gap.

Keywords : Terahertz spectroscopy, Metamaterials
OCIS codes : (300.6495) Spectroscopy, terahertz; (160.3918) Metamaterials; (160.4670) Optical materials

I. INTRODUCTION

Metamaterials have attracted great interest because they exhibit light-matter interactions distinct from those of natural materials; some of these distinctive features are negative refraction, superlensing, cloaking, perfect absorption, and target-material sensing [1-6]. Metamaterials consist of an array of metallic structures that interact with electromagnetic waves; many types of structures have been suggested, including split-ring resonators that operate across a wide range of frequencies [7-10]. Various resonance modes appear in metamaterials, such as inductive-capacitive (*LC*), dipole, and quadrupole resonances. In particular, the *LC* resonance is typically characterized by its frequency $f_0 = 1/(2\pi\sqrt{LC})$, where L is the inductance of the side-arm structure and C is the capacitance of the gap structure [11]. Most significantly, the *LC* resonance frequency can be shifted by changing the effective capacitance, *e.g.* by manipulating the dielectric configuration around the gap.

Recently, THz metamaterials have emerged as a potential platform for sensing microorganisms at low concentrations in ambient and aqueous environments [5, 12]. The detection volume of a metasensor is strongly confined to the region near its surface; hence, a very thin water layer minimizes the attenuation losses present in THz wave transmission in aqueous environment [13]. In addition, for sensing applications, the effect of the geometrical parameters on the metamaterial resonance has to be addressed in fuller detail, to optimize the devices; these factors include the gap width, effective substrate index, and edge roughness of the metal pattern [14, 15]. Obviously, design details of the gap in metamaterial sensors are crucial to optimizing their operation; for instance, the vertical extent of the sensing volume in conjunction with the gap width has recently been addressed [16]. However, the sensitivity as a function of the relative position of the target substance has not been studied explicitly.

In this research, we used terahertz time-domain spectroscopy (THz-TDS) to study how the specific location of the target substance on the metamaterial affects its sensitivity. We first functionalized the gap area of the metamaterial by coating it with an adhesive polymer; the result is that polystyrene (PS) spheres are captured preferentially in that region. We studied the resonance-frequency shift of the

*Corresponding author: ahny@ajou.ac.kr, ORCID 0000-0002-8563-076X
Color versions of one or more of the figures in this paper are available online.

THz metamaterials as a function of the position of the dielectric spheres, which was reproduced by the sensitivity distribution simulated by a finite-difference time-domain (FDTD) method.

II. RESULTS AND DISCUSSION

To demonstrate enhanced sensitivity, it is crucial to concentrate the target substances into the gap area of the THz metamaterial, because the effective sensing interaction is highly confined there [14, 17-21]. To that end, we functionalized the gap region with a poly-*L*-lysine (PLL) polymer that works as an adhesive layer; the target materials were captured only around the effective area (Fig. 1) [22, 23]. As shown in Fig. 1(a), we spin-coated a hexamethyl-disilazane (HMDS) layer and then a negative-tone photoresist (Ma-N 1420, Microchem Inc.) onto a Si substrate. Specific regions of the photoresist and HMDS layers were then removed through developing and UV-ozone treatment respectively. The PLL solution was dispensed onto the sample, incubated for 15 minutes at room temperature, and subsequently blown dry using nitrogen gas. We removed the remaining photoresist layer through a lift-off process in acetone, with an ultrasonic treatment for 15 s. The final functionalized devices had a PLL layer exposed in the gap area only, while covered elsewhere by an HMDS layer that worked as an anti-adhesive layer. Figure 1(b) shows a dark-field microscopy image of the periodic pattern of PS spheres deposited on the PLL-patterned Si substrate (with a thickness of 550 μm), without the metamaterial patterns. The size of the PS spheres was 850 nm; they were deposited by dipping the patterned Si substrate in a solution containing the spheres for 10 min. The image confirms that the PS spheres were attached predominantly in the PLL regions, while they were not found in other regions where the HMDS had been coated. We also patterned the same PLL and HMDS layers onto the THz metamaterials, as shown in Fig. 1(c). The metamaterials were fabricated on a Si substrate (with a thickness of 550 μm) by employing a conventional photolithography technique, followed by metal evaporation of Cr/Au (2 nm/98 nm). The THz metamaterials consist of an electrical split-ring resonator with a side-arm length of 36 μm (*l*), a line width of 4 μm (*w*), a gap width of 3 μm (*d*), and a periodicity of 50 μm [5]. To capture the target materials in the gap area only, we functionalized the gap region of the THz metamaterials through the process shown in Fig. 1(a). After being dipped in the PS solution, the PS beads are collected very effectively near the gap area only, as we can clearly identify. THz spectra were recorded by using a homemade THz-TDS system with an acquisition time of 5 s [24, 25].

To provide direct evidence that the localization of the target materials is crucial, we performed THz-TDS experiments on the functionalized metamaterials, as shown in Fig. 2. We prepared two different configurations of metamaterial arrays with localized PLL polymer coatings. For the device shown in Fig. 2(a), the PLL layer was coated at the center of the gap, and as a result the PS spheres were located around the gap area after the dipping process. In contrast, for the second sensor configuration (Fig. 2(b)) the PLL coating was located 10 μm away from the gap center, and the PS spheres were located outside the gap area. The transmission spectra of the PS-coated metamaterials (red lines) are plotted in Figs. 2(c) and 2(d) for the gap-centered and offset cases (Figs. 2(a) and 2(b)), respectively. Transmission spectra for uncoated metamaterials are also shown for comparison (black lines).

As mentioned above, the metamaterial resonance changes when dielectric materials are deposited on the surface, because of the change in the effective index of the gap region. The resonance-frequency shift can be described

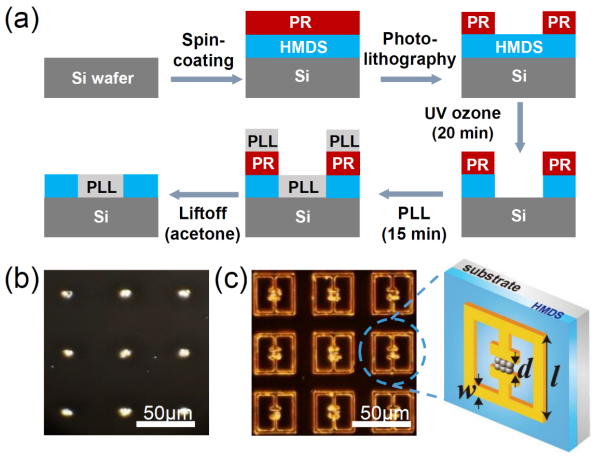

FIG. 1. (a) Schematic for fabricating the functionalized device. (b) Dark-field microscopy image of the periodic pattern of polystyrene (PS) sphere deposited on the PLL-patterned Si substrate. (c) Dark-field microscopy image of metamaterial (functionalized with PLL) after PS deposition.

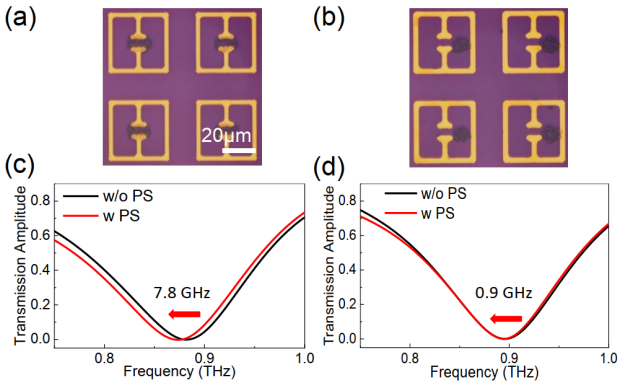

FIG. 2. Microscopy image of the metamaterial with PS spheres coated (a) onto the center of the gap, and (b) outside the gap area. (c) and (d): Experimental transmission spectra for the metamaterial array, corresponding to the PS locations in (a) and (b) respectively.

approximately by the relationship $\Delta f/f_0 \approx -\alpha N_{av}(\varepsilon_p - \varepsilon_{air})/\varepsilon_{eff}$ [5, 6, 13], where α is a coefficient, N_{av} is the surface density of target materials, ε_p and ε_{air} are the dielectric constants of polystyrene spheres and air respectively, and ε_{eff} is the effective dielectric constant without the target substances. As expected, the PS deposition at the center of the gap causes the resonance frequency to shift toward the red, due to the increased effective dielectric constant in the gap area [5, 6, 8, 12]; the measured frequency shift is $\Delta f = 7.8$ GHz (Fig. 2(c)). However, the shift for the PS coating outside the gap area is $\Delta f = 0.9$ GHz (Fig. 2(d)), smaller than the in-gap case. We note that because the PS coated area is relatively large, some of the PS spheres may have overlapped with the effective sensing area. Here the effective dielectric constant can be determined by a combination of air and substrate indices, resulting in $\varepsilon_{eff} = 6.4$ for the Si substrate [26, 27]. The number of PS spheres located in the gap area was around 30 on average; in other words, the surface density was 0.012 μm^{-2}, if divided by the entire unit cell area of 50×50 μm^2. Therefore, the coefficient in terms of surface number density of PS was estimated to be $\alpha = 3.02$ μm^2/particle, whereas it will vary depending on the size of PS.

We performed FDTD simulations (Lumerical) to confirm our experimental results and quantify the position-dependent sensitivity of the metamaterials [12]. For target materials, we placed dielectric spheres with a diameter of 1 μm in a 3×7 array, and used the dielectric constant of polystyrene ($\varepsilon_p = 2.56$) [28]. The transmission spectra with the PS (red lines) and without (black lines) are shown in Figs. 3(a) and 3(b) respectively. The shift Δf is much larger (6.9 GHz) when the beads are located at the center of the gap.

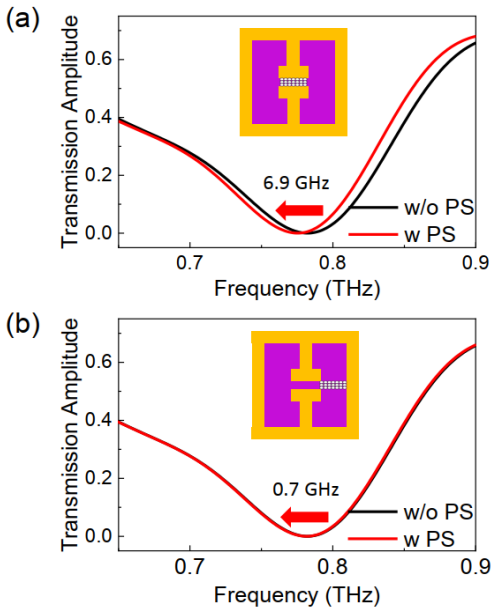

FIG. 3. FDTD simulation results for dielectric spheres coated (a) on the center of the gap, (b) outside the gap area.

Significantly, Δf is much smaller (0.7 GHz) when they are located away from the gap. Again, this confirms the crucial role of the gap structure in sensing with metamaterials.

Finally, to obtain the sensitivity distribution for our metamaterial pattern, we carried out an FDTD simulation of the frequency shift to determine its dependence on the position of the target materials, shown in Fig. 4, because Δf is proportional to the sensitivity, according to $S = \Delta f / N_{av}$ [6]. We chose a dielectric cube with an edge length of 1 μm and a dielectric constant of $\varepsilon_p = 10$ as the target material (Fig. 4(a)). Figure 4(b) shows the representative transmission spectra from the simulation when the dielectric cube was located in the gap area (in particular, near the edge of the metal gap structure). We note that the resonant frequency is higher (1.29 THz) relative to those in Figs. 2 and 3, in which we used a Si substrate. Quartz substrate is beneficial because the frequency shift is higher in the case of lower substrate index [12]. Clearly, the two-dimensional (2D) distribution for Δf illustrates a unique sensitivity map that is strongly localized around the gap area (Fig. 4(c)). Only marginal frequency shifts are observed outside the gap area (except for some regions near the metal edges). Significantly, we find that the sensitivity is particularly high near the metal edge within the gap area: The shift is 2.4 times as great near the metal edge as at the center of the gap. For comparison, we plot the 2D distribution of electric field amplitude (E_y) in the x-y plane (at $z = 0$) for a device with a gap width of 3.0 μm (Fig. 4(d)). As discussed above, the effective detection volume of the THz metamaterial in the gap area is highly confined near the surface, which is indicated by the electric field being strongly confined

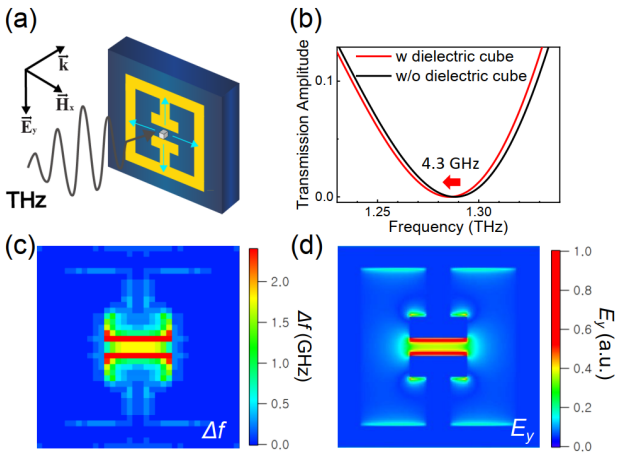

FIG. 4. (a) Schematic of position-dependent sensitivity mapping by using FDTD simulation. (b) Simulated transmission spectra for the metamaterials on a quartz substrate, with and without the presence of a dielectric cube (1 μm^3) located in the gap area. (c) Simulation showing 2D mapping of the resonance-frequency shift (color bar, in GHz) as a function of the dielectric cube's position. (d) 2D plot of the electric field (E_y) distribution at the resonance frequency of 1.29 THz.

around the gap area. In particular, the field distribution matches nicely with the sensitivity map shown in Fig. 4(c), including the fact that the sensitivity is enhanced near the metal edge.

III. CONCLUSION

In conclusion, we investigated the position-dependent sensitivity of THz metamaterials by using localized concentrations of PS microbeads. A shift of the metamaterial's resonance frequency occurred when we coat the microbeads on the gap area by using PLL functionalization; however, the frequency shift is negligible when we deposited them on other areas of the metamaterial. A FDTD simulation reproduced our experimental findings successfully. Finally, to infer the sensitivity distribution from the simulation, we calculated the frequency shift as a function of the position of a target dielectric cube, using a step size of 1 μm. The resultant 2D mapping of the frequency shift clearly demonstrated that the sensitivity was higher for target positions inside the gap area, particularly near the edge of the metal pattern. This result was consistent with the 2D distribution of electric field, which was highest near the metal edge. This will help us to find the optimal conditions for the high-sensitivity sensing of target materials.

ACKNOWLEDGMENT

The authors acknowledge support from the Midcareer National Research Foundation of Korea (NRF) (2017R1A2 B4009177) and the Korea Institute of Energy Technology Evaluation and Planning (KETEP) (20184030202220).

REFERENCES

1. R. A. Shelby, D. R. Smith, and S. Schultz, "Experimental verification of a negative index of refraction," Science **292**, 77-79 (2001).
2. I. I. Smolyaninov, Y. J. Hung, and C. C. Davis, "Magnifying superlens in the visible frequency range," Science **315**, 1699-1701 (2007).
3. J. B. Pendry, D. Schurig, and D. R. Smith, "Controlling electromagnetic fields," Science **312**, 1780-1782 (2006).
4. N. I. Landy, S. Sajuyigbe, J. J. Mock, D. R. Smith, and W. J. Padilla, "Perfect metamaterial absorber," Phys. Rev. Lett. **100**, 207402 (2008).
5. S. J. Park, J. T. Hong, S. J. Choi, H. S. Kim, W. K. Park, S. T. Han, J. Y. Park, S. Lee, D. S. Kim, and Y. H. Ahn, "Detection of microorganisms using terahertz metamaterials," Sci. Rep. **4**, 4988 (2014).
6. S. J. Park, S. H. Cha, G. A. Shin, and Y. H. Ahn, "Sensing viruses using terahertz nano-gap metamaterials," Biomed. Opt. Express **8**, 3551-3558 (2017).
7. H. T. Chen, W. J. Padilla, J. M. O. Zide, A. C. Gossard, A. J. Taylor, and R. D. Averitt, "Active terahertz metamaterial devices," Nature **444**, 597-600 (2006).
8. J. F. O'Hara, R. Singh, I. Brener, E. Smirnova, J. Han, A. J. Taylor, and W. Zhang, "Thin-film sensing with planar terahertz metamaterials: Sensitivity and limitations," Opt. Express **16**, 1786-1795 (2008).
9. J. Federici and L. Moeller, "Review of terahertz and subterahertz wireless communications," J. Appl. Phys. **107**, 111101 (2010).
10. W. Cao, R. Singh, I. A. I. Al-Naib, M. He, A. J. Taylor, and W. Zhang, "Low-loss ultra-high-Q dark mode plasmonic Fano metamaterials," Opt. Lett. **37**, 3366-3368 (2012).
11. J. D. Baena, J. Bonache, F. Martín, R. M. Sillero, F. Falcone, T. Lopetegi, M. A. G. Laso, J. García-García, I. Gil, M. F. Portillo, and M. Sorolla, "Equivalent-circuit models for split-ring resonators and complementary split-ring resonators coupled to planar transmission lines," IEEE Trans. Microw. Theory Tech. **53**, 1451-1461 (2005).
12. S. J. Park, B. H. Son, S. J. Choi, H. S. Kim, and Y. H. Ahn, "Sensitive detection of yeast using terahertz slot antennas," Opt. Express **22**, 30467-30472 (2014).
13. S. J. Park, S. A. N. Yoon, and Y. H. Ahn, "Dielectric constant measurements of thin films and liquids using terahertz metamaterials," RSC Adv. **6**, 69381-69386 (2016).
14. J. T. Hong, D. J. Park, J. H. Yim, J. K. Park, J. Y. Park, S. Lee, and Y. H. Ahn, "Dielectric constant engineering of single-walled carbon nanotube films for metamaterials and plasmonic devices," J. Phys. Chem. Lett. **4**, 3950-3957 (2013).
15. J. T. Hong, S. W. Jun, S. H. Cha, J. Y. Park, S. Lee, G. A. Shin, and Y. H. Ahn, "Enhanced sensitivity in THz plasmonic sensors with silver nanowires," Sci. Rep. **8**, 15536 (2018).
16. S. J. Park, S. A. N. Yoon, and Y. H. Ahn, "Effective sensing volume of terahertz metamaterial with various gap widths," J. Opt. Soc. Korea **20**, 628-632 (2016).
17. T. J. Yen, W. J. Padilla, N. Fang, D. C. Vier, D. R. Smith, J. B. Pendry, D. N. Basov, and X. Zhang, "Terahertz magnetic response from artificial materials," Science **303**, 1494-1496 (2004).
18. M. A. Seo, H. R. Park, S. M. Koo, D. J. Park, J. H. Kang, O. K. Suwal, S. S. Choi, P. C. M. Planken, G. S. Park, N. K. Park, Q. H. Park, and D. S. Kim, "Terahertz field enhancement by a metallic nano slit operating beyond the skin-depth limit," Nat. Photonics **3**, 152-156 (2009).
19. Y. T. Chang, Y. C. Lai, C. T. Li, C. K. Chen, and T. J. Yen, "A multi-functional plasmonic biosensor," Opt. Express **18**, 9561-9569 (2010).
20. A. Berrier, P. Albella, M. Ameen Poyli, R. Ulbricht, M. Bonn, J. Aizpurua, and J. G. Rivas, "Detection of deep-subwavelength dielectric layers at terahertz frequencies using semiconductor plasmonic resonators," Opt. Express **20**, 5052-5060 (2012).
21. T. Chen, S. Li, and H. Sun, "Metamaterials application in sensing," Sensors **12**, 2742-2765 (2012).
22. K. Colville, N. Tompkins, A. D. Rutenberg, and M. H. Jericho, "Effects of poly (L-lysine) substrates on attached escherichia coli bacteria," Langmuir **26**, 2639-2644 (2010).
23. P. Laurino, R. Kikkeri, N. Azzouz, and P. H. Seeberger, "Detection of bacteria using glyco-dendronized polylysine prepared by continuous flow photofunctionalization," Nano

Lett. **11**, 73-78 (2011).
24. S. J. Park, A. R. Kim, J. T. Hong, J. Y. Park, S. Lee, and Y. H. Ahn, "Crystallization kinetics of lead halide perovskite film monitored by in situ terahertz spectroscopy," J. Phys. Chem. Lett. **8**, 401-406 (2017).
25. H. S. Kim, S. H. Cha, B. Roy, S. H. Kim, and Y. H. Ahn, "Humidity sensing using THz metamaterial with silk protein fibroin," Opt. Express **26**, 33575-33581 (2018).
26. D. J. Park, J. T. Hong, J. K. Park, S. B. Choi, B. H. Son, F. Rotermund, S. Lee, K. J. Ahn, D. S. Kim, and Y. H. Ahn, "Resonant transmission of terahertz waves through metallic slot antennas on various dielectric substrates," Curr. Appl. Phys. **13**, 753-757 (2013).
27. D. J. Park, S. J. Park, I. Park, and Y. H. Ahn, "Dielectric substrate effect on the metamaterial resonances in terahertz frequency range," Curr. Appl. Phys. **14**, 570-574 (2014).
28. G. Zhao, M. T. Mors, T. Wenckebach, and P. C. M. Planken, "Terahertz dielectric properties of polystyrene foam," J. Opt. Soc. Am. B **19**, 1476-1479 (2002).